Thin-Walled Structures 47 (2009) 1457–1468

Contents lists available at ScienceDirect

Thin-Walled Structures

journal homepage: www.elsevier.com/locate/tws

Stiffened panel stability behaviour and performance gains with plate prismatic sub-stiffening

D. Quinn [a], A. Murphy [a,*], W. McEwan [a], F. Lemaitre [b]

[a] School of Mechanical and Aerospace Engineering, Queen's University Belfast, Ashby Building, Belfast. Northern Ireland BT9 5AH, UK
[b] Unité Aéronautique et Laminés Technique, Centre de Recherche de Voreppe, Centr'Alp, BP 27, 38341 Voreppe Cedex, France

ARTICLE INFO

Article history:
Received 8 January 2009
Received in revised form
15 July 2009
Accepted 15 July 2009
Available online 08 August 2009

Keywords:
Panel buckling
Sub-stiffening
Machined panels
Panel testing

ABSTRACT

To increase the structural efficiency of integrally machined aluminium alloy stiffened panels, it is plausible to introduce plate sub-stiffening to increase the local stability and thus panel static strength performance. Reported herein is the experimental validation of prismatic sub-stiffening, and the computational verification of such concepts within larger recurring structure. The experimental work demonstrates the potential to 'control' plate buckling modes. For the tested sub-stiffening design, an initial plate buckling performance gain of +89% over an equivalent mass design was measured. The numerical simulations, modelling the tested sub-stiffening design, demonstrate equivalent behaviour and performance gains (+66%) within larger structures consisting of recurring panels.

1. Introduction

1.1. Background

Aircraft stiffened panel structure, which is moderately loaded and as a result has 'thin' plate elements, is designed in such a way that local buckling of the plates between lateral and longitudinal stiffeners is allowed to occur at a fraction of the load required to cause panel collapse. This post-buckling strength capacity has significant potential for structural weight savings. In addition, recent advances in the strength and damage tolerance characteristics of aerospace metallic materials [1,2], offers further opportunity for increased panel working and limit stresses. To maximise these material improvements as weight savings on aircraft primary structures, it is desirable to enhance panel stability further. Improved panel structural efficiency is plausible by introducing plate element sub-stiffening [3]. In addition to potential panel stability improvements, sub-stiffening also has the potential to improve damage tolerance capabilities [4–6]. The concept of plate element sub-stiffening for static strength performance gains relies on the introduction of structural features which modify the initial plate buckling mode. This concept has yet to be fully validated experimentally and potential aircraft applications evaluated. Consequently this paper documents a combined experimental and numerical research programme undertaken to examine static strength performance gains attained with sub-stiffening on representative aircraft panels. Work is currently underway on advanced manufacturing methods, including welding, and non-prismatic sub-stiffening concepts under uniform compression and combined compression and shear loading. The global research objective is to assess the potential for plate sub-stiffening and develop the required design and analysis tools to allow the introduction of sub-stiffening in aircraft panel design.

1.2. Advanced manufacturing processes and materials

Traditionally, airframes are constructed with complete wing and fuselage components built-up from individually fabricated sub-components. To date, riveted assembly of stiffened panel sub-components has dominated in metallic airframes. A potential alternative is to manufacture sub-components as integral structures. The advantage of single piece integral panels over fabricated structures is the potential for cost savings associated with assembly labour and tooling [7,8]. The NASA 'Integral Airframe Structures' program [9] indicated that, as compared to conventional built-up fabrication methods, high-speed machining designs could yield recurring cost savings of 61%. Additionally, life cycle cost savings are possible through reduced part count for both the Original Equipment Manufacturer (OEM) and aircraft operator.

1.3. Panel sub-stiffening

One of the first applications of plate sub-stiffening was to improve fatigue crack growth in integral structures. In built-up

* Corresponding author. Tel.: +44 28 9097 4095; fax: +44 28 9066 1729.
E-mail address: a.murphy@qub.ac.uk (A. Murphy).

0263-8231/$ - see front matter © 2009 Elsevier Ltd. All rights reserved.
doi:10.1016/j.tws.2009.07.004

structures, attached stiffeners act as crack arresters restraining the propagation of fatigue crack growth. Conventional integral panel structures, however, do not have natural breaks to act as crack arresters and therefore fatigue crack propagation through an integral structure is potentially faster. The introduction of plate sub-stiffening can be shown to significantly decrease fatigue crack growth under constant amplitude loading [5]. Considering static strength, Bushnell and Rankin [10] demonstrated that including small sub-stiffeners between the conventional primary stiffeners can 'not only lead to an increased buckling resistance, but more importantly to a much more robust optimum in terms of stiffener pitch'. Murphy et al. [3] experimentally and computationally examined plate sub-stiffening, demonstrating potential combined performance gains for both initial plate buckling and panel post-buckling collapse. In more recent work, Watson et al. [11] applied the exact finite strip method to investigate 'extra' buckling modes which occur when sub-stiffeners or multiple stiffener sizes are introduced in stiffened panel designs. As with Bushnell and Rankin, it was found that mass savings are achieved by using stiffeners of more than one size and there is the potential for increased spacing of the primary longitudinal and transverse stiffeners.

1.4. Paper synopsis

The work presented herein is part of a larger research program which is investigating potential sub-stiffening concepts, manufacturing methods and developing design and analysis tools. The experimental work is focused at the sub-component level, examining multi stiffener panels between transverse stiffeners. Additional numerical studies focus on sub-component and component levels. The experimental work is validated before expanding the numerical analyses to evaluate potential performance gains when applied within larger panel structure. The present study focuses on prismatic sub-stiffening concepts for structures loaded under uniform compression, with specimen manufacture focused on integral machining. The following paper section provides an overview of the induced physical behaviour of panels with plate sub-stiffening. Having introduced the behaviour, the following section introduces the design of the experimental specimens considered herein. This is followed with details on the applied experimental and computational analysis procedures. The experimental data is presented, followed by results from the numerical investigation. The results are discussed and the paper concludes with a summary of the findings.

2. Panel stability

2.1. Conventional panel stability

2.1.1. Initial plate buckling

Stiffened panels are essentially an assemblage of plate and column elements. Plate sections, bounded by lateral and longitudinal stiffeners, behave according to plate theory with edge boundary conditions defined by the rotational rigidity of the bounding stiffeners. Considering for simplicity a flat rectangular plate, of uniform thickness, simply supported on all sides and under uniform compressive loading—the critical buckling load is given by

$$N_x = \frac{\pi^2 a^2 D}{m^2}\left(\frac{m^2}{a^2}+\frac{n^2}{b^2}\right)^2 \tag{1}$$

where

$$D = \frac{E\cdot t^3}{12(1-\nu^2)} \tag{2}$$

and a, b and t are the plate geometric properties (length, breadth and thickness respectively), E and ν are the material properties (Young's modulus and Poisson's ratio respectively) and m and n define the buckle waveform (m equalling the number of longitudinal half-waves and n equalling the number of lateral half-waves).

Now assuming typical aerospace lateral and longitudinal stiffener pitches and therefore plate element aspect ratios, the plate will buckle with one or more half-waves in the longitudinal direction and a single half-wave in the lateral direction. The relationship can then be reduced to

$$(N_x)_{m\geq 1,n=1} = \frac{\pi^2\cdot D}{a^2}\left(m+\frac{1}{m}\frac{a^2}{b^2}\right)^2 \tag{3}$$

Then given a particular instance of a plate (fixed material and geometric properties), the relationship between the number of longitudinal half-waves (m) and the plate buckling stress can be examined, Fig. 1. On a conventional aircraft stiffened panel, where plate bays buckle with one lateral half-wave and m longitudinal half-waves, for strength assessment the value of m which generates the lowest critical stress, m_{critical}, is of key importance.

2.1.2. Post-buckling stability

Stiffened panel post-buckling stability is dictated by stiffener column behaviour. Longitudinal stiffener sections, in addition to a portion of the plate on either side, act as effective columns. According to Von Karmen [12], the width of the post-buckled effective plate is defined as

$$b_{\text{Effective}} = b\sqrt{\frac{\sigma_{\text{Buckle}}}{\sigma_{\text{Stiffener}}}} \tag{4}$$

where σ_{Buckle} is the stress at which the plate element initially buckles and $\sigma_{\text{Stiffener}}$ is the stress at the plate edge when the post-buckling effective stiffener column becomes unstable.

Stiffened panel collapse is a result of instability of the effective stiffener column. Critical stiffener instability stress may be determined using the secant formula, Eq. (5), with failure

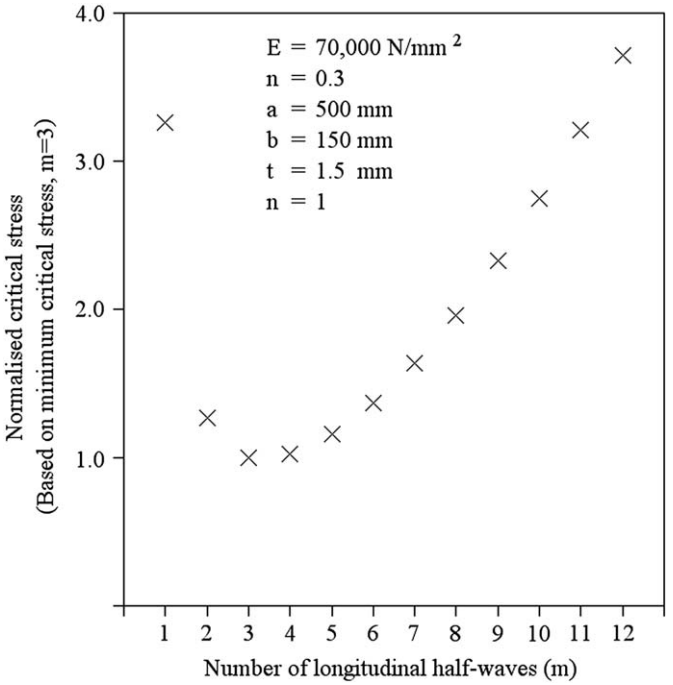

Fig. 1. Normalised compressive buckling stress for a flat rectangular plate simply supported on all edges.

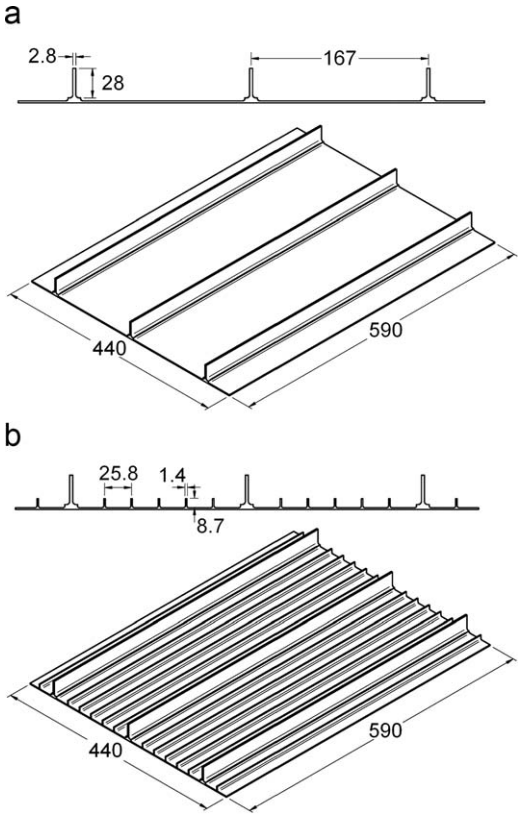

Fig. 2. Test specimen geometry. (a) Specimen A; (b) Specimen B.

Table 1
Specimen design masses.

	Mass (kg)	Designed mass percentage difference (%)
Specimen A	1.959	–
Specimen B	1.968	+0.459

occurring when a critical stress level, σ_{Max}, is reached. This critical stress can be based on a local material yielding value or a local stiffener element instability value. Further details on the initial buckling and post-buckling failure analysis of stiffened panels may be found in [12–14].

$$\sigma_{Max} = \sigma_{Column}\left[1 + \frac{ey}{\rho^2}\,\mathrm{Sec}\left[\frac{L'}{2\rho}\sqrt{\frac{\sigma_{Column}}{E_t}}\right]\right] \quad (5)$$

2.2. Sub-stiffening hypothesis

The objective of plate sub-stiffening herein is to improve initial panel stability performance and positively increase the ultimate collapse performance of the structure. Considering the relationship between plate buckling load and the number of longitudinal half-waves, Fig. 1, if the number of longitudinal half-waves could be 'controlled', then to increase plate performance, a value of m, which was either greater or smaller than $m_{critical}$, would be desirable. To increase the number of longitudinal half-waves, additional transverse stiffening would be required to introduce node lines across the plate. To decrease the number of longitudinal half-waves, structural features would have to be added to the plate to prevent square half-waves forming. Such features would have to force the central line of the plate to behave like a column, forming a single longitudinal half-wave buckle. An alternative view would be that the addition of such sub-stiffening structural features would result in a non-isotropic plate bending stiffness. This would not only alter the stress at which buckling occurred but would also change the form of instability, resulting in an increased or decreased number of half-waves. In essence, with either approach, the plate element would become a stiffened panel within the larger stiffened panel. In terms of design, such an approach introduces more variables and therefore the potential for greater optimisation and tailoring and hence, as noted in the literature, the potential for more robust optimums in terms of primary stiffener pitches.

Table 2
Specimen manufactured masses.

	Mass (kg)	Percentage difference from design mass (%)	Manufactured mass percentage difference (%)
Specimen A	2.008	+2.50	–
Specimen B	1.981	+0.66	−1.34

Focusing on compression critical panel design, introducing features which longitudinally stiffen would offer more overall benefit than adding features which would provide further transverse stiffening. In addition, examining Fig. 1 and the performance gain per change in buckle half-wave, the greatest performance gain for the minimum buckle pattern alteration would be via a reduction in the number of half-waves. Hence, the introduction of longitudinal sub-stiffeners is of great interest, assuming they could be designed to force the plate centre line to behave like a column. Buckling with a single longitudinal half-wave assuming simply supported loading ends or as a full wave (two edge section quarter-waves and one central half-wave) assuming clamped loading ends.

Considering panel post-buckling, improved plate stability may be translated into improved collapse performance. Higher initial plate buckling stresses alone may result in improved load carrying ability of the plate bays. In addition, while considering the post-buckling effective plate, Eq. (4), higher initial buckling stresses may result in stronger effective columns with higher critical stresses. Two important issues need consideration if such an approach is to be viable:

(a) Any sub-stiffener/primary stiffener combination must be designed such that the potential for unstable interaction of modes is prevented. The potential for mode coupling with local and overall buckling modes is well known. The so called 'naive optimum' is extremely imperfection sensitive and can result in significantly premature failure.
(b) Any sub-stiffener/plate combination must offer a static strength performance gain over a constant thickness plate design. However, in order to add any sub-stiffeners to the plate design without increasing the total material volume and therefore mass, would require a reduction in the plate thickness. This would only be possible in panel design scenarios where reductions of plate thickness would not violate fatigue, damage tolerance or minimum thickness constraints. However, as noted in the introduction, new materials offer opportunities for increased panel working and limit stresses.

Considering the issues outlined above, the key objective of the present work is therefore to introduce longitudinal sub-stiffeners within a panel design without increasing material volume and

experimentally validate the 'control' of initial plate buckling modes without degrading post-buckling potential.

3. Experimental analysis

3.1. Specimen design

The baseline specimen design was constrained to aerospace representative panel loading intensities and initial buckling to collapse strength ratios. A specimen configuration of three longitudinal stringers was selected for compatibility with previous work. The selected configuration resulted in two central plate bays and two edge plate bays separated by the stiffeners, Fig. 2. Given the target panel loading intensity and buckling to collapse strength ratio, the cross-section of the longitudinal stiffeners and the central plate sections were sized. The edge plate bay geometry was then defined such that initial plate buckling of the edge bays would occur at a marginally higher stress level than that required for the central bays. Experimentally this arrangement stops the premature failure of the specimen edge stiffeners. Finally, given the generated geometry and the selected manufacturing method, integral machining from thick plate, available material stock size and basic damage tolerance constraints, the design was fine-tuned.

Given the final design of the baseline specimen (Specimen A), a number of initial sub-stiffening configurations were studied. A number of manufacturing and minimum thickness and maximum height constraints were applied to the initial configurations and a single prismatic configuration was selected for detailed design. The selected configuration resulted in a reduction of the baseline plate thickness to allow the introduction of five blade section sub-stiffeners within each central plate bay. Based on the selected prismatic sub-stiffening configuration, a final specimen design considering machining and damage tolerance constraints was developed. The final sub-stiffened specimen design is given in Fig. 2 (Specimen B). Given the applied machining and damage tolerance constraints, it was not possible to have identical specimen masses and meet all other design constraints. Hence Specimen B's design is marginally heavier than Specimen A's, Table 1.

The specimens were manufactured on a Bridgeport VMC 1000/22, programmed using FeatureCam. They were machined from 50-mm-thick Aluminium Alloy 2024-T351 plate. Once manufactured all specimen dimensions were measured to assess machining accuracy. The specimen plate sections, primary and sub-stiffeners were scanned for initial geometric imperfection patterns and each specimen was accurately weighed. Table 2 details the manufactured specimen masses. Examining both the global and local specimen machined geometry, the increase in mass over the designed masses relates to slightly thicker plate and stiffener dimensions. This was directly related to machinist experience and as Specimen A was manufactured first the oversized thicknesses are more significant.

Both specimens exhibited approximately similar geometric imperfections, with a single half sine wave along the length of the specimen in the stiffener direction and a single half sine wave across the width of the specimen. Both Specimens A and B's imperfections are 'stiffener-out', that is to say the specimen plate imperfection is convex. Analysing the magnitude of the curvature parallel to the primary stiffeners—the maximum out-of-plane magnitude is 10.5% of the plate thickness measured from the specimen edge to the specimen centre for Specimen A and 26.3% for Specimen B (percentage based on Specimen A's plate element thickness for consistency). It is clear that the manufacturing induced imperfection for Specimen B is larger than that of Specimen A. This coupled with the marginally larger cross-sectional area of Specimen A, should advantage the baseline specimen in the experimental results.

3.2. Experimental procedure

The specimens were tested in a 500 kN capacity hydraulic testing machine. A reinforced epoxy resin base (42 mm thick) was cast on to each specimen loading end, producing clamped boundary conditions. Once cast each specimen was marked and strain gauged in preparation for test. Gauges were located to assist in the determination of initial plate buckling and post-buckling collapse behaviour. Two calibrated displacement transducers, one either side of the specimen, were used to measure specimen end-shortening.

To capture plate behaviour during test, a three-dimensional Digital Image Correlation (DIC) system was used (VIC-3D, Correlated Solutions). The DIC method allows the determination of the deformation and therefore strains by cross correlating successive images of the specimen acquired during the test. The specimen is viewed by a pair of high resolution, digital CCD cameras and a random pattern with good contrast applied to the specimen plate. The deformation of the plate is then recorded at set time intervals during the test by the cameras and the data post processed once the test is completed to evaluate plate surface deformation and strain behaviour. The specimens were loaded monotonically, in displacement control, at a rate of 0.40 mm/min until failure occurred. Load, deflection, strain data and DIC images were recorded automatically at 2 s intervals.

4. Computational analysis

Accurate modelling of stiffened panel initial plate buckling and post-buckling collapse behaviour is achievable through the use of the finite element method and employing non-linear material and geometric analysis procedures [15].

4.1. Idealisation

To accurately capture the buckling failure modes of the stiffened panels, they must be idealised as an assemblage of shell elements [16]. For all finite element models presented herein, stiffeners and plate sections are represented using mid-plane shell elements, connected by rigid link Multi Point Constraints [17] between geometrically offset regions [3].

4.2. Element and mesh selection

Applying the element selection and mesh convergence procedures outlined in Murphy et al. [18] the four-noded quadrilateral, thin shell element S4R [17] were selected for the finite element simulations. With the selected element, the convergence study defined a minimum mesh density of six nodes per buckle half-wave for the structural configurations under investigation. The final mesh for each analysis was defined considering the minimum mesh density and the desire to have a consistent mesh pattern across the complete simulation series.

4.3. Simulation classes

Two simulation classes were created and analysed. The first represented the experimental test conditions with the appropriate specimen geometry and experimental boundary conditions. The purpose of these simulations was to validate the applied finite

Table 3
Experimental initial plate buckling and ultimate panel collapse loads.

	Initial plate buckling load (kN)	Ultimate panel collapse load (kN)
Specimen A	74.5	216.6
Specimen B	140.2	255.0

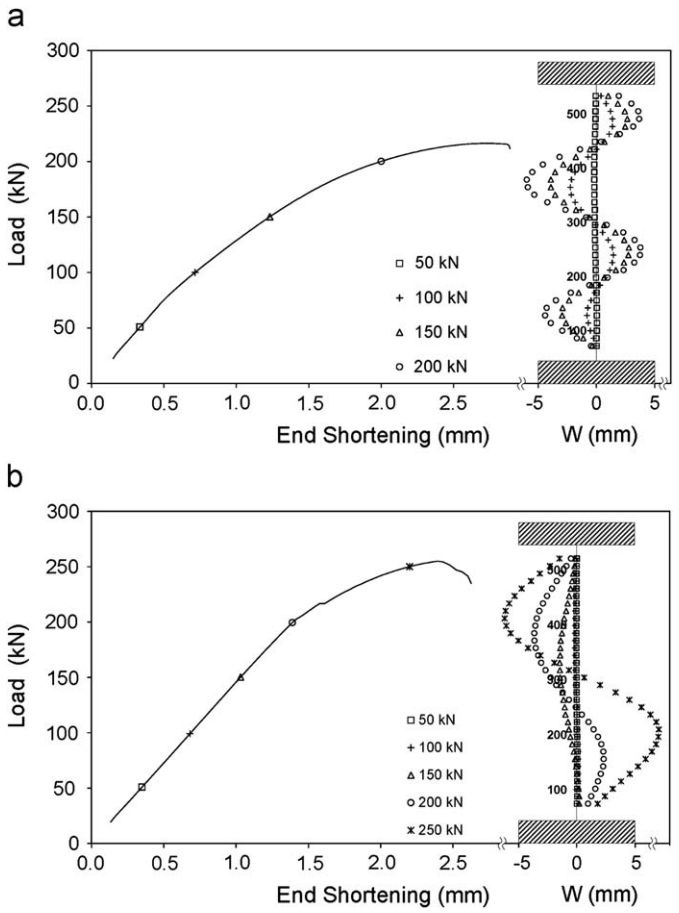

Fig. 3. Experimental load versus end-shortening curves along with out-of-plane deformation data for the centre line of the right hand central plate bay (with the panel viewed from its un-stiffened side) at selected load levels. (a) Specimen A; (b) Specimen B.

element idealisation and analysis procedures. The second class of simulations represented equivalent panel and sub-stiffener geometry but applied to a larger panel structure, unaffected or constrained by experimental boundary conditions. The purpose of these simulations was to expand the experimental knowledge by computationally examining sub-stiffening within larger recurring panel structures and thereby verify behaviour and performance levels.

4.3.1. Simulation procedure validation (experimental models)

The validation models were designed to be as representative of the experimental test setup as possible. To model the test specimen support bases, the out-of-plane displacements of the nodes within the areas that were cast in epoxy resin in the experimental tests were restrained. To represent specimen loading, an uniform axial displacement was applied to the lower end of the models, while the axial displacement at the opposite end was restrained, again in the axial direction. Finally, the specimen's unloaded edges were left free in space, corresponding with the experimental setup.

4.3.2. Large panel sub-stiffening verification (recurring panel models)

These simulations applied the validated idealisation and analysis procedures from the preceding analysis. Equivalent panel cross-sectional geometries were considered, however for these simulations the models represented four longitudinal stiffener bays and three lateral stiffener bays. As with the previous simulations, uniform axial displacement (in the primary stiffener direction) was used to apply the model load (at the lower end of the models) and equivalent restraint at the opposite end reacted this loading. The lateral stiffeners were represented with simple support constraints at the lateral stiffener locations and at the models unloaded edges periodic boundary conditions were applied with appropriate rotational restraints.

4.4. Material modelling

A series of through-thickness material test coupons were extracted from the aluminium alloy thick plate from which the specimens were manufactured. A total of eighteen coupons, at six equally spaced through-thickness locations, were extracted by wire Electro Discharge Machining. This allowed the detailed through-thickness material definition of the original thick plate. The generated material data was then idealised as Ramberg–Osgood curves allowing its direct inclusion within the simulations (using the "classical metal plasticity" constitutive theory available within the ABAQUS material library [17]). The experimentally measured data highlighted a variation in material properties with thick plate through-thickness location. To determine the sensitivity of the simulation predictions to the variation in through-thickness material properties, a study was conducted with three varying fidelity material definitions, all based on the experimentally determined data.

The study was conducted with the experimental geometry and boundary conditions of Specimen A and using an eigen-mode imperfection. All simulations predicted similar initial buckling and collapse behaviour, with maximum variation in initial buckling and collapse load of 3.2% for the various material definitions. The chosen material definition involves the reduction of the experimental through-thickness data, by volume weighted averaging, to three materials, each corresponding to key panel structural features (primary stiffeners, sub-stiffeners, plate elements).

4.5. Imperfection modelling

Modelling of initial imperfections is of great importance when evaluating panel stability behaviour [15,18–20]. Therefore, the out-of-plane distortions of the experimental specimens in their test conditions were accurately measured using a Co-ordinate Measuring Machine (CMM). This data allowed the characterisation and comparison of individual specimen imperfections. In addition, the measurement of the individual specimen distortion allowed the inclusion of the actual test specimen geometric imperfections within the appropriate computational simulations.

The inclusion of the measured imperfection within the computational simulations required a two-step analysis. In the first step, the perfect mesh of the test specimen is distorted by way of a nodal displacement static analysis to match the experimentally measured imperfection. In the second step, a stress free version of the mesh is used to perform the collapse analysis. For simulations where no measured imperfection is

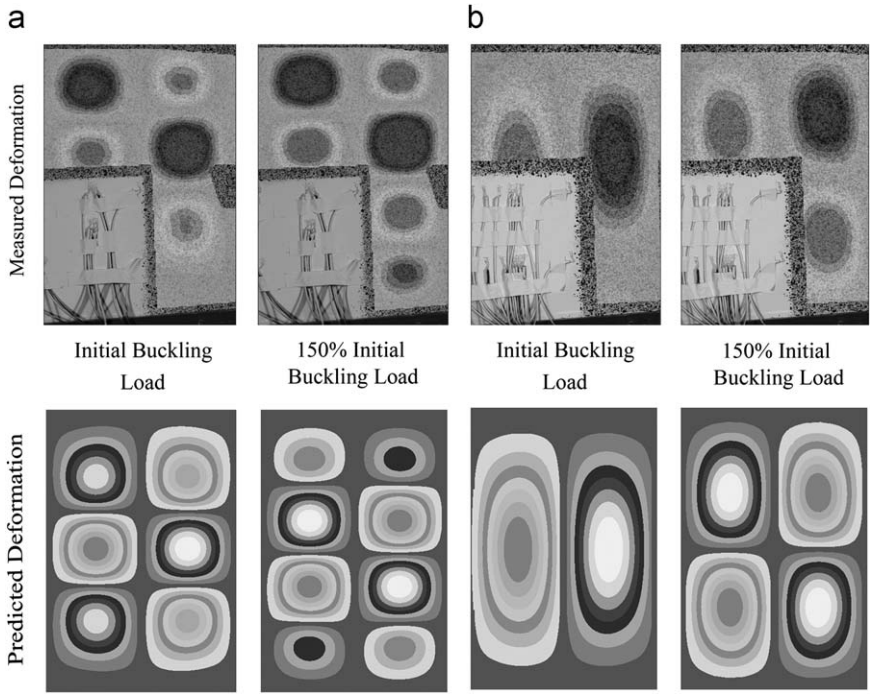

Fig. 4. Experimental and predicted out-of-plane deformations for Specimens A and B central skin bays.

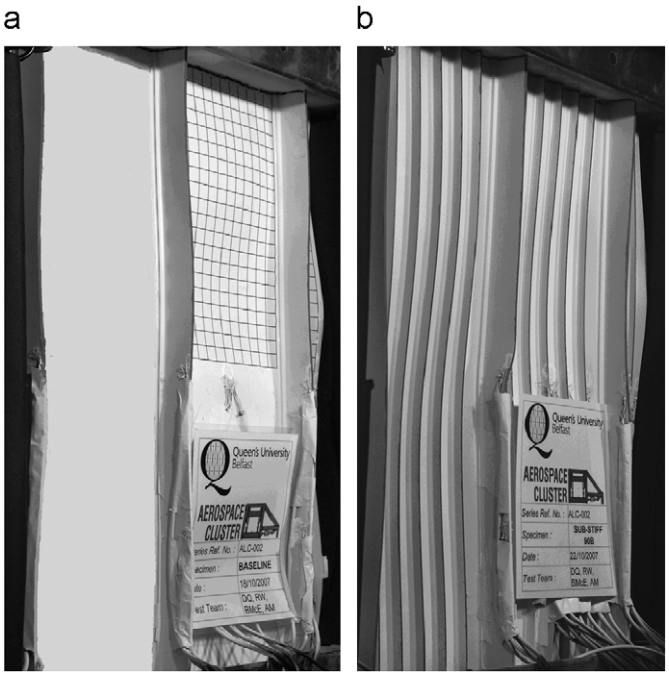

Fig. 5. Specimen collapse modes. (a) Specimen A; (b) Specimen B.

available (i.e. the large panel sub-stiffening verification models), the perfect simulation mesh is seeded with an eigen-mode, typically the first mode and with a magnitude associated with the employed manufacturing method.

4.6. Solution procedure

For all computational analysis, the incremental-iterative Newton–Raphson solution procedure in which the applied load is broken down into a series of load increments is utilised [21].

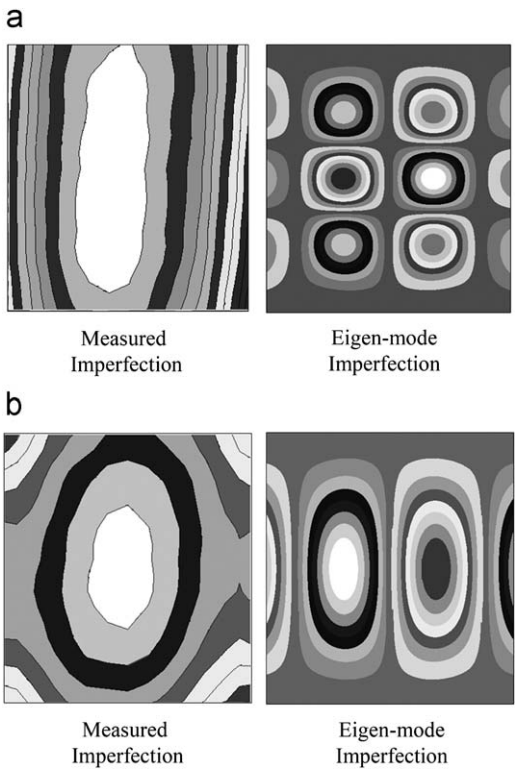

Fig. 6. Specimen imperfections. (a) Specimen A; (b) Specimen B.

5. Results and discussion

5.1. Experimental results

Table 3 presents the experimentally measured initial plate buckling and ultimate panel collapse loads for Specimens A and B. For the determination of initial plate buckling, the parabolic strain

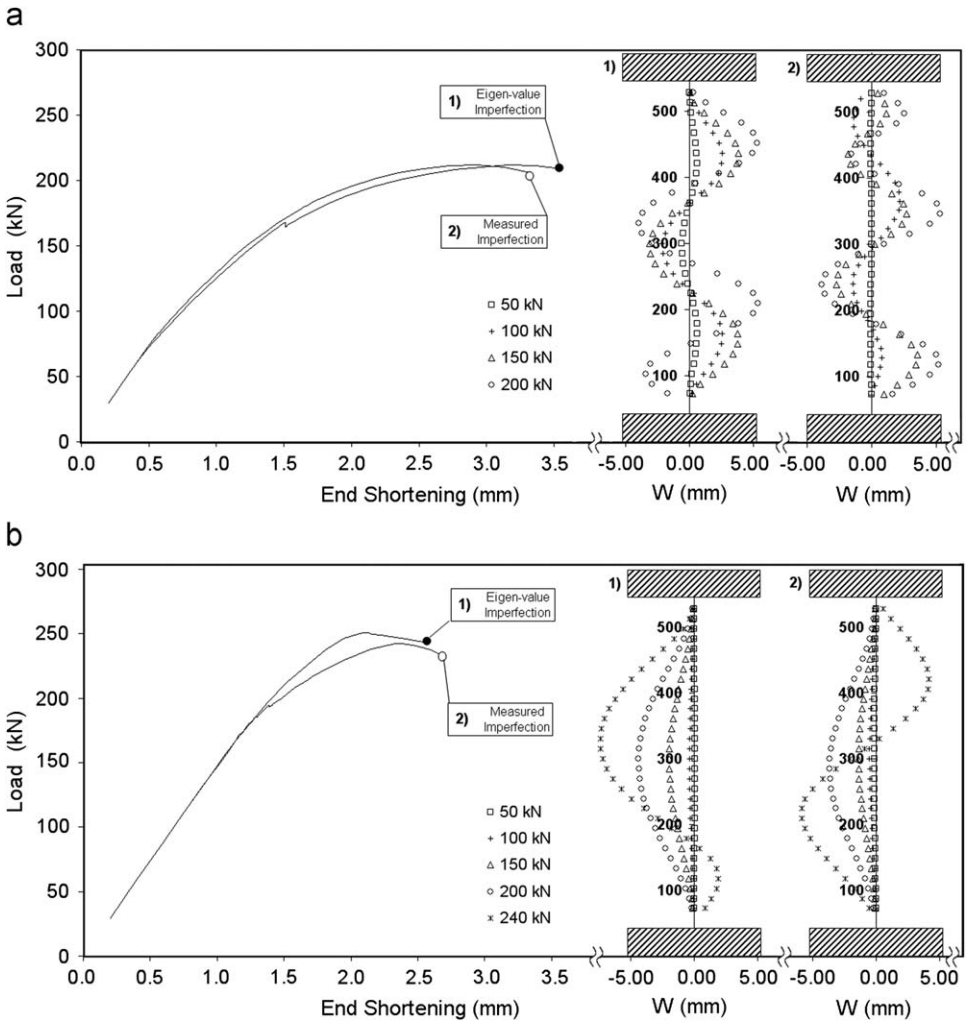

Fig. 7. Predicted Specimen load versus end-shortening curves seeded with (1) measured initial geometric imperfections and (2) fundamental eigen-mode initial geometric imperfection.

Table 4
Computationally predicted initial plate buckling and ultimate panel collapse loads for the experimental specimens.

	Specimen A		Specimen B	
	Initial plate buckling load (kN)	Ultimate panel collapse load (kN)	Initial plate buckling load (kN)	Ultimate panel collapse load (kN)
Experimental data	74.5	216.6	140.2	255.0
Measured imperfection	78.2	212.1	144.5	242.6
Eigen-mode imperfection	52.8	211.7	138.0	250.9

differential method [22] was used with strain data from back-to-back gauges located at the same point on both specimens (the centre of the left hand central plate bay, with the panel viewed from its un-stiffened side), Fig. 4. Fig. 3 presents the load versus end-shortening curves, illustrating specimen pre- and post-buckling stiffness. Additionally, Fig. 3 also illustrates out-of-plane deformation data for the centre line of the right hand central plate bay (with the panel viewed from its un-stiffened side) at selected load levels. Fig. 4 presents fringe plots of both specimen initial and evolved plate buckle modes.

5.1.1. Specimen A

Specimen initial plate buckling occurred at 74.5 kN, 34% of the specimens ultimate collapse load, with the central plate bays buckling anti-symmetrically into three longitudinal half-waves. For this specimen, there was a plate post-buckling mode change at 42% of the specimens ultimate collapse load, when fourth half-waves developed, more or less simultaneously, in each of the central bays (Fig. 3). In each plate bay, these four half-waves continued to grow in out-of-plane magnitude until the specimen collapsed. Considering specimen collapse, failure was by way of combined global stiffener flexure (stiffener-in) and local material yielding (Fig. 5).

5.1.2. Specimen B

For this specimen, the central plate bays initially buckled with single longitudinal half-waves at 140.2 kN (55% of the specimens maximum load), Fig. 4. Examining the DIC out-of-plane deformation

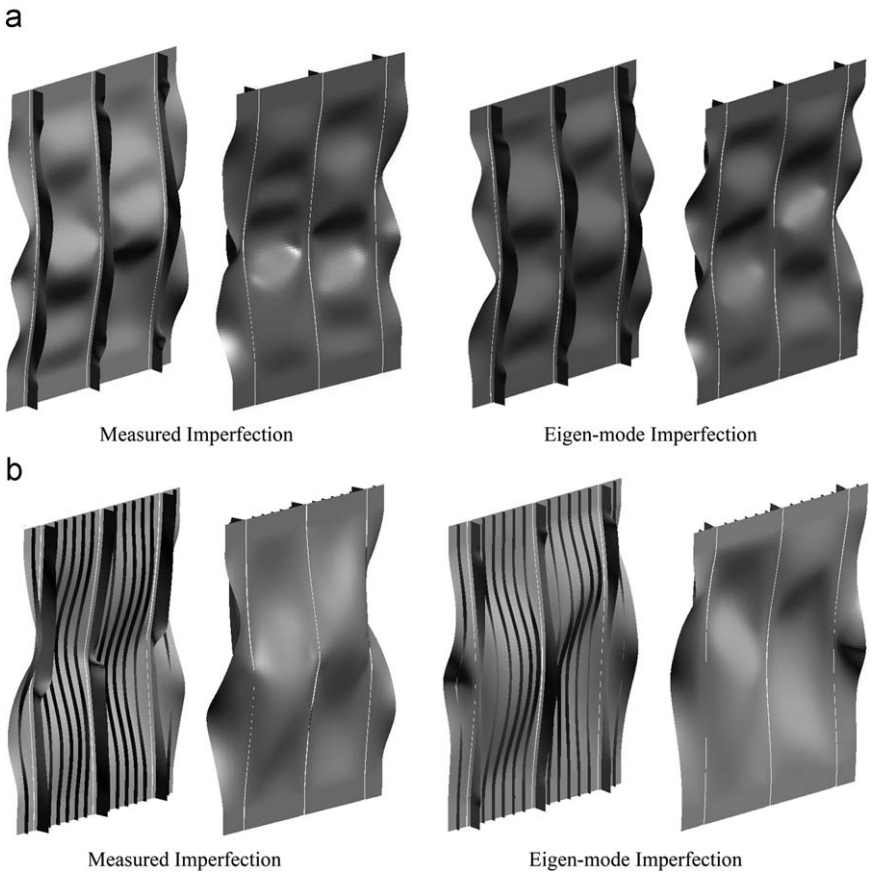

Fig. 8. Specimen simulation predicted collapse modes. (a) Specimen A; (b) Specimen B.

data for the right hand central plate bay (with the panel viewed from its un-stiffened side), Fig. 4, an additional half-wave formed from the bottom at 199.5 kN (78% of the specimens maximum load). The additional half-wave grew steadily from its detection until the specimen collapsed, causing the original half-wave to reduce in length, Figs. 3 and 4. Considering the left hand central plate bay (with the panel viewed from its un-stiffened side), the strain gauge data indicates similar behaviour, with an initial central longitudinal half-wave buckle evolving into two half-waves at 216.7 kN (85% of the specimens maximum load), Fig. 4. For this sub-stiffened specimen, collapse involved failure of the central stiffener with a combined global stiffener flexure (stiffener-out) and local web crippling mode (Fig. 5).

5.2. Computational results—experimental models

To assess the influence of initial geometric imperfections on the simulation predictions, models were seeded with both measured imperfections and eigen-mode imperfections, Fig. 6. The predicted load versus end-shortening curves obtained for both imperfection types and for both specimens is presented in Fig. 7. Table 4 presents the computationally predicted initial plate buckling and ultimate panel collapse loads. As with the experimental analysis, initial plate buckling was determined applying the parabolic strain differential method with strain data from back-to-back virtual gauges located at the same point on all specimens and models (the centre of the left hand central plate bay, with the panel viewed from its un-stiffened side). Fig. 4 presents the predicted out-of-plane plate behaviour for both specimen models seeded with measured imperfections.

5.2.1. Specimen A

Both simulations accurately predicted the number of initial buckle half-waves. The simulation seeded with the eigen-mode imperfection predicted an overly conservative buckling load (−29%), whereas the simulation seeded with the measured imperfection marginally over predicted the initial buckling performance (+5%). Considering post-buckling behaviour, the use of the measured imperfections allows accurate prediction of mode changes observed experimentally. With the simulation predicting an increase in the number of half-waves from three to four at 85.5 kN (40% collapse load). In the case of the eigen-mode seeded simulation, a mode change from three to four half-waves is predicted but not until 165 kN (78% collapse load).

Considering specimen collapse, both simulations produce conservative predictions within 2.3% of those experimentally measured (measured imperfection simulation −2.1%, eigen-mode imperfection simulation −2.3%). The measured imperfection simulation shows good agreement with the experimental results for final end-shortening at collapse (+5.0%). In the case of the eigen-mode seeded analyses, the simulation over predicts the specimen final end-shortening at collapse by +15.8%. The predicted failure mode of both the eigen-mode and measured imperfection analysis are consistent, displaying global stiffener flexure (stiffener-in) with local material yielding (Fig. 8).

5.2.2. Specimen B

As with Specimen A, both simulations accurately predict the number of initial buckle half-waves. The simulation seeded with the eigen-mode imperfection marginally under predicts the initial buckling load (−2.1%), whereas the simulation seeded with the measured imperfection marginally over predicts the specimen

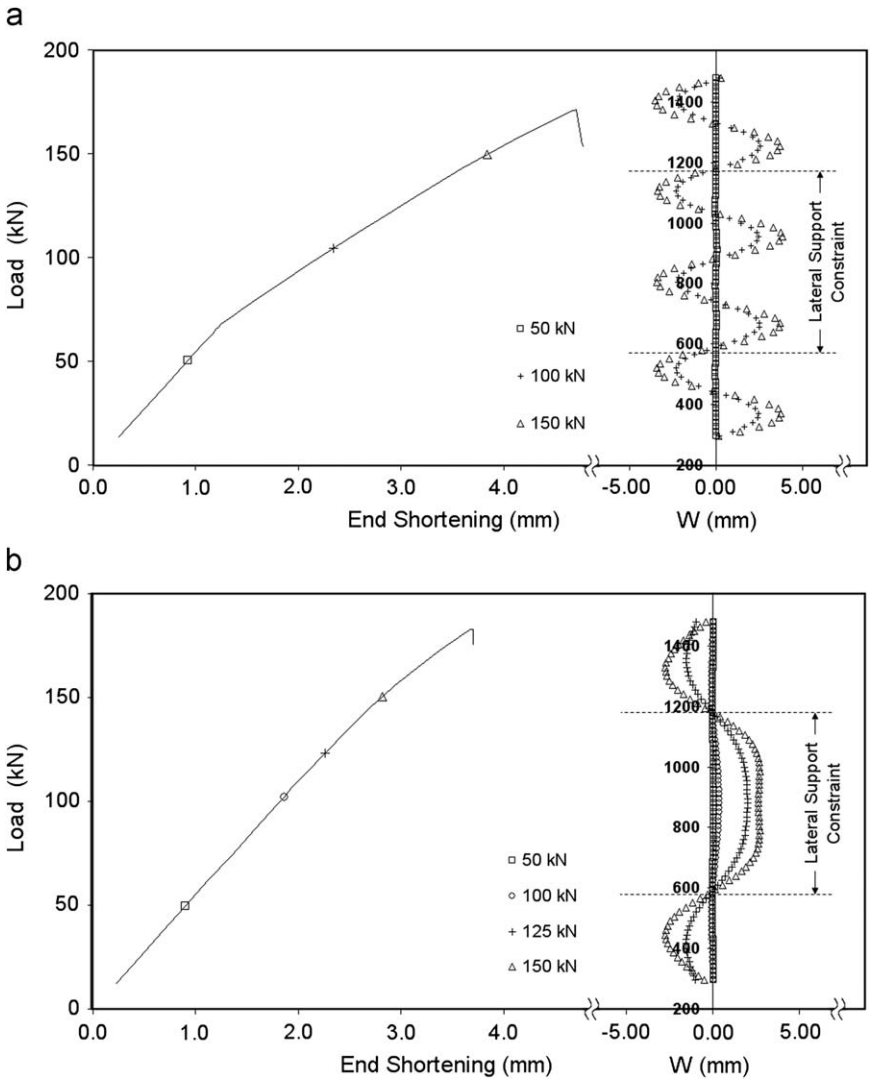

Fig. 9. Recurring panel models load versus end-shortening curves. (a) Design A; (b) Design B.

initial plate buckling performance (+2.6%). Again, the use of the measured imperfection provides accurate prediction of mode changes observed experimentally, with the simulation predicting an increase from one to two half-waves in each central bay at 186 and 193 kN (78% and 85% of the collapse load respectively). In the case of the eigen-mode seeded analyses, a mode change from one to two half-waves is predicted, but this is predicted to occur at 97% and 99% of the specimen collapse load.

Studying specimen collapse, both simulations produce conservative predictions, with the measured imperfection simulation under predicting by −4.8%, and the eigen-mode imperfection simulation under predicting by −1.9%. The measured imperfection simulation shows good agreement with the experiment final end-shortening at collapse (−0.4%). In the case of the eigen-mode seeded analyses, the simulation under predicts the specimen final end-shortening at collapse by −12.6%. The prediction of the Specimen B's failure mechanism varies with seeded initial imperfection. The measured imperfection simulation is in agreement with experimental data, i.e. global stiffener flexure (stiffener-out) with local web crippling (Fig. 8). The predicted failure mode with the eigen-mode simulations is global stiffener flexure (stiffener-in) with localised material yielding (Fig. 8).

5.3. Computational results—recurring panel models

As no experimental imperfection data is available for the recurring panel structures, the simulations are seeded with eigen-mode imperfections. The predicted load versus end-shortening curves obtained for the recurring panel simulations are represented in Fig. 9. Design A represents the constant plate thickness cross-sectional geometry of Specimen A, and, Design B represents the sub-stiffened plate cross-sectional geometry of Specimen B. Table 5 presents the computationally predicted initial plate buckling and ultimate panel collapse loads. Again, the determination of initial plate buckling employs the parabolic strain differential method with strain data from back-to-back virtual gauges located at the centre of the left hand central plate bay, with the model viewed from its un-stiffened side. Fig. 10 presents the predicted initial plate buckling out-of-plane fringe plots in addition to simulation predicted collapse modes.

5.3.1. Design A

The simulation predicts initial plate bay buckling with four plate half-waves at 61.5 kN (36% of the ultimate collapse load)

(Fig. 10) and predicts that this plate buckle waveform is maintained until collapse. Considering collapse, the simulation predicts ultimate failure as global stiffener flexure (stiffener-in) with local yielding (Fig. 10), with this occurring at 171.3 kN.

5.3.2. Design B

For Design B the simulation predicts initial buckling with a single plate half-wave, occurring at 102.0 kN (56% of the ultimate collapse load) (Fig. 10). This initial plate buckling formation is maintained, as with Design A, until collapse of the panel. The simulation predicts ultimate failure at 182.9 kN with a global stiffener flexure (stiffener-out) with a local yielding mode (Fig. 10).

Table 6 summarises the key measured and predicted, design and specimen loads and modes.

5.4. Discussion

5.4.1. Initial plate buckling behaviour

Examining the experimental results, it can be seen that the initial buckling form of a panel plate elements may be modified with the addition of sub-stiffeners. These sub-stiffeners can, without adding mass to the panel structure, improve initial plate buckling performance and therefore positively influence overall post-buckling collapse strength. It is worth noting that the initial longitudinal half-wave mode shapes of the sub-stiffened plates were only temporarily stable. As specimen loading increased above the buckling load, the single longitudinal half-wave buckles evolved into two half-wave buckles before the specimen finally collapsed. Examining the finite element predictions of the test specimens, there is excellent agreement with the experimental behaviour when the actual test specimen measured imperfections are represented within the models. Initial plate buckling forms are predicted accurately with the associated load being marginally over predicted, possibly due to the absence of initial specimen residual stresses. Initial buckling predictions seeded with the eigen-mode imperfections closely mirror the experimental behaviour but are consistently conservative. Applying the validated computational techniques, the understanding of sub-stiffening was computationally expanded to larger structures consisting of recurring panels. These simulations demonstrate equivalent initial buckling behaviour and performance gains for sub-stiffening within larger recurring panel structures, unaffected by experimental boundary conditions.

Table 5
Computationally predicted initial plate buckling and ultimate panel collapse loads for the recurring panel models.

	Design A		Design B	
	Initial plate buckling load (kN)	Ultimate panel collapse load (kN)	Initial plate buckling load (kN)	Ultimate panel collapse load (kN)
Eigen-mode imperfection	61.5	171.3	102.0	182.9

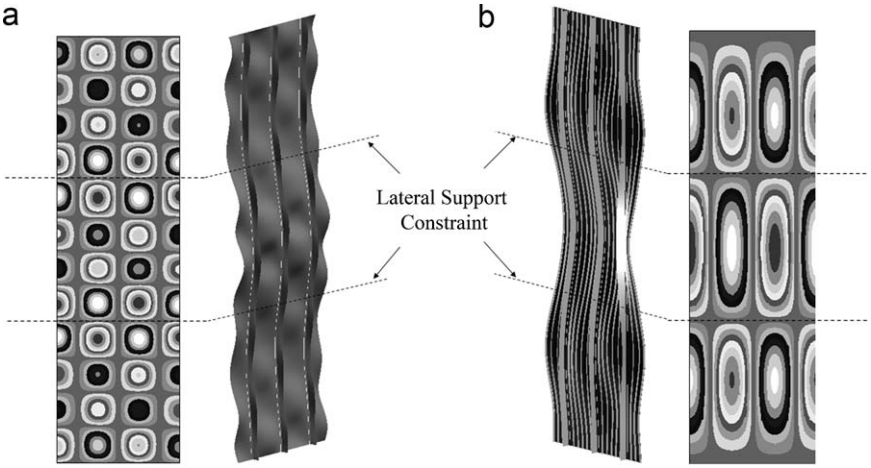

Fig. 10. Recurring panel models predicted initial buckling out-of-plane deformations and final collapse modes. (a) Design A; (b) Design B.

Table 6
Key measured and predicted, design and specimen loads and modes.

	Initial skin bay buckling		First skin bay mode jump		Ultimate specimen/design collapse	
Experiment/simulation	Load (kN)	Mode	Load (kN)	Mode	Load (kN)	Mode
Specimen A	74.5	$m=3$	91.0	$m=4$	216.6	Stiffener flexure plus local material yielding
Simulation of Specimen A (measured imperfection)	78.2	$m=3$	85.5	$m=4$	212.1	Stiffener flexure plus local material yielding
Simulation of Specimen A (Eigen-mode Imperfection)	52.8	$m=3$	165.0	$m=4$	211.7	Stiffener flexure plus local material yielding
Simulation of design A (eigen-mode imperfection)	61.5	$m=4$	n/a	n/a	171.3	Stiffener flexure plus local material yielding
Specimen B	140.2	$m=1$	199.5	$m=2$	255.0	Stiffener flexure plus local web crippling
Simulation of Specimen B (measured imperfection)	144.5	$m=1$	186.0	$m=2$	242.6	Stiffener flexure plus local web crippling
Simulation of Specimen B (eigen-mode imperfection)	138.0	$m=1$	243.4	$m=2$	250.9	Stiffener flexure plus local material yielding
Simulation of design B (eigen-mode imperfection)	102.0	$m=1$	n/a	n/a	182.9	Stiffener flexure plus local material yielding

5.4.2. Collapse behaviour

Considering experimental specimen collapse, the sub-stiffened specimen failed in a dissimilar manner to the conventional specimen. The greater longitudinal initial geometric imperfection associated with the sub-stiffened design may have influenced the 'stiffener-out' direction of collapse. It should also be noted that the sub-stiffeners remain stable through to failure, only bending in their own plane in response to the plate buckle form. The post-buckling and collapse behaviour of the experimental specimens were predicted closely when simulations represented the specimen measured imperfections. In these cases, plate buckle mode changes and collapse loads were predicted within 5% of those experimentally measured. For the simulations with eigen-mode imperfections, the experimental post-buckling behaviour was less accurately predicted. Mode changes, while predicted, were different in form and tended to be predicted at higher loads than were measured experimentally.

Finally, the variation in measured primary stiffener initial imperfection between the conventional and sub-stiffened specimens appears to have affected predicted failure modes. Considering the conventional specimen (Specimen A), where the stiffener initial imperfection is relatively small, predictions using a measured imperfection and the eigen-mode imperfection are similar, and as a result failure mechanisms are in agreement with each other and the experimental data. However, the initial primary stiffener geometric imperfection for the sub-stiffened specimen (Specimen B) is larger in magnitude. Predictions seeded with the measured imperfection replicates this deformation, whereas the predictions seeded with the eigen-mode imperfection does not. Consequently, this may have contributed to the inability of the eigen-mode imperfection simulation to predict closely the collapse behaviour of Specimen B.

5.4.3. Mass optimised design

Considering the potential performance gains achieved for the mass equivalent specimens, the validated finite element methods were utilised to convert performance gains into potential mass savings. A specimen redesign was undertaken, focused on modifying the skin bay geometry whilst holding the global panel dimensions and primary stiffener geometry constant. The resulting design, matched the initial buckling and collapse performance of the baseline design (Specimen A), but with a significantly reduced mass (−15.6%). Examining the variation between the ''mass optimised'' and mass equivalent (Specimen B) design, the mass optimised design exhibits a reduced number of sub-stiffening blades per central bay (four rather than five), with the blades marginally higher and thicker than the mass equivalent design, with ultimately a reduced skin bay thickness.

6. Conclusions

To increase the structural efficiency of integrally machined aluminium alloy stiffened panels, it is plausible to introduce plate sub-stiffeners to increase the local plate stability and thus panel stability.

- The experimental work focused on the sub-component level and examined prismatic sub-stiffening concepts under uniform compression. To this end, two aluminium alloy specimens were designed, manufactured and tested with the same primary stiffener configuration and primary stiffener cross-section designs, as well as the same global length, width and near identical masses. The sub-stiffener designs were heavily constrained with manufacturing and damage tolerance minimum thickness and maximum height constraints. The experimental work demonstrates the potential to 'control' plate buckling modes to improve panel stability. For the particular geometry and material tested, an initial plate buckling performance gain of 87.2% and resultant panel post-buckling collapse gain of 17.7% was found.
- Numerical studies of the validation specimens indicate that, using measured material and initial geometric imperfections, behaviour of sub-stiffened components can be predicted accurately. Initial buckling and collapse loads were predicted within 5% of experimental data.
- Further numerical studies aimed to evaluate if equivalent behaviour and performance gains are achievable when applied to larger structures consisting of recurring panels. Expansion of original specimen designs to larger panel structures suggest that the ability to maintain control of initial buckle forms is possible with associated gains of 65.9% and 6.8% observed for initial buckling and collapse performance.

Acknowledgement

The authors gratefully acknowledge the technical and financial support of Alcan CRV, Voreppe, France.

References

[1] Knuewer M, Schumacher J, Ribes H, Eberl F, Bes B. 2198 Advanced aluminium lithium alloy for A350 skin sheet application. In: Proceedings of the seventeenth advanced aerospace materials & processes conference and exposition (AeroMat 2006). Seattle, USA: 15–18 May 2006.
[2] Lequeu P, Dif R, Warner T, Dumont D, Wood P. New solutions for lightweight upper wing skins of large airframes. In: Proceedings of the sixteenth advanced aerospace materials & processes conference and exposition (AeroMat 2005). Orlando, USA: 6–9 June 2005.
[3] Murphy A, Quinn D, Mawhinney P, Ozakça M, van der Veen S. Tailoring static strength performance of metallic stiffened panels by selective local sub-stiffening. In: Proceedings of the forty seventh AIAA/ASME/ASCE/AHS/ASC structures, structural dynamics, and materials conference. Newport, Rhode Island: 1–4 May 2006, AIAA-2006-1944.
[4] Farley GL, Newman JA, James MA. Selective reinforcement to improve fracture toughness and fatigue crack growth resistance in metallic structures. In: Proceedings of the forty fifth AIAA/ASME/ASCE/AHS/ASC structures, structural dynamics & materials conference. Palm Springs, California: 19–22 April 2004, AIAA 2004-1924.
[5] Ehrström J-C, Van der Veen S, Arsène S, Muzzolini R. Improving damage tolerance of integrally machined panels. In: Proceedings of the twenty third symposium of international committee on aeronautical fatigue (ICAF 2005). Hamburg, Germany: 6–10 June 2005.
[6] Boscolo M, Allegri G, Zhang X. Design and modeling of selective reinforcements for integral aircraft structures. AIAA J September 2008;46(9).
[7] Pettit RG, Wang JJ, Toh C. Validated feasibility study of integrally stiffened metallic fuselage panels for reducing manufacturing costs. NASA Contractor Report, May 2000, NASA/CR-2000-209342.
[8] Metschan S. Validated feasibility study of integrally stiffened metallic fuselage panels for reducing manufacturing costs, cost assessment of manufacturing/design concepts. NASA Contractor Report, February 2000, NASA/CR-2000-209343.
[9] Munroe J, Wilkins K, Gruber M. Integral airframe structures (IAS)—validated feasibility study of integrally stiffened metallic fuselage panels for reducing manufacturing costs. NASA Contractor Report, May 2000, NASA/CR-2000-209337.
[10] Bushnell D, Rankin C. Optimum design of stiffened panels with sub-stiffeners. In: Proceedings of the forty sixth AIAA/ASME/ASCE/AHS/ASC structures, structural dynamics & materials conference. Austin, Texas: 18–21 April 2005, AIAA 2005-1932.
[11] Watson A, Featherston CA, Kennedy D. Optimization of post-buckled stiffened panels with multiple stiffener sizes. In: Proceedings of the forty eighth AIAA/ASME/ASCE/AHS/ASC structures, structural dynamics, and materials conference. Honolulu, Hawaii: 23–26 April 2007, AIAA 2007-2207.
[12] Bruhn EF. Analysis and design of flight vehicle structures, 1st ed.. Tri-State Offset Company; 1973.
[13] NASA. NASA astronautics structures manual, Vol. 3. Washington, US: NASA; 1961.
[14] ESDU structures sub-series, Engineering Sciences Data Units, ESDU International Ltd.
[15] Lynch C, Murphy A, Price M, Gibson A. The computational post-buckling analysis of fuselage stiffened panels loaded in compression. Thin-Walled Struct 2004;42(10):1445–64.

[16] Domb MM, Elliott WG, Leigh BR. Modelling of stiffener crippling phenomena using finite element analysis. Can Aeronaut Space J 1998;44(4):256–62.
[17] Anonymous. ABAQUS—version 6.5 user's manual. Hibbitt, Karlsson and Sorenson, Inc.; 2004.
[18] Murphy A, Price A, Gibson A. Toward Virtual Testing of Airframe Stiffened Panels. In: Proceedings of the royal aeronautical society—virtual testing conference. Hamilton Place, London. 25–26 October 2006, Day 1, Paper 3.
[19] Hu SZ, Jiang L. A finite element simulation of the test procedure of stiffened panels. Mar Struct 1998;11:75–99.
[20] Baker DJ, Kassapoglou C. Post-buckled composite panels for helicopter fuselages: design, analysis, fabrication and testing, presented at the American Helicopter Society, Hampton roads chapter, structures specialists meeting, Williamsburg VA US, October 2001.
[21] Becker AA. Understanding non-linear finite element analysis—through illustrative benchmarks, 1st ed.. NAFEMS; 1-8743-7635-2.
[22] Singer J, Arbocz J, Weller T. Buckling experiments: experimental methods in buckling of thin-walled structures, 1st ed.. New York (Chichester, UK): Wiley; 1997.